Follicular delivery of a novel peptide therapeutic for the treatment of androgenic alopecia

By

K. Ryan Moulder

Submitted to the graduate degree program in Bioengineering and the Graduate Faculty of the University of Kansas in partial fulfillment of the requirements for the degree of Master of Science.

_____

Chairperson Dr. M. Laird Forrest

_____

Dr. Teruna Siahaan

_____

Dr. Prajnaparamita Dhar

Date Defended: December 2, 2015

The Thesis Committee for K. Ryan Moulder certifies that this is the approved version of the following thesis:

Follicular delivery of a novel peptide therapeutic for the treatment of androgenic alopecia

_____

Chairperson Dr. M. Laird Forrest

Date approved: December 2, 2015

Abstract

Androgenic alopecia (AGA), commonly known as pattern baldness, along with "loss of hair" following chemotherapy induced alopecia (CIA) are widespread maladies with treatments of little to no effectiveness. Following the discovery of a novel 4.2-kDa peptide's (murikal/SPR4) ability to markedly increase hair growth when injected intradermally in wild type mice, liposomal topical formulations were developed and optimized to facilitate greater follicular delivery of the therapeutic peptide. Significant enhancement of hair growth rate was seen in mice treated with the peptide and liposomal vehicle when compared to commercial minoxidil (Rogaine®) formulations and peptide alone. An array of lipid formulations and preparation protocols were screened for follicular penetration efficiency utilizing biotinylated or fluor-labeled peptide and confocal microscopy. Two lead formulations were selected for a month long stability study of particle and peptide integrity. Each lead formulation showed near constant retention of encapsulated peptide. Formulation 3 showed a steady profile of ideal particle characteristics, particle size (~300 nm) and zeta potential (~70 mV), over the time period and temperatures tested. The two lead formulations were also applied ex-vivo to donor human scalp skin to determine translatability to a human follicle anatomy. Results of confocal microscopy imaging of treated human tissue were inconclusive on peptide penetration and follicle localization. Further testing is required to demonstrate translatability to human tissues. Overall, these results indicate the clear therapeutic potential of murikal formulated into an optimized liposomal solution for the treatment of AGA and CIA.

Acknowledgements

First, I would like to thank my advisor Dr. Laird Forrest for his guidance and support in this project. He has given me the opportunity to grow as a scientist and entrepreneur with this research and for that I am forever grateful. Thank you to Dr. Teruna Siahaan and Dr. Prajnaparamita Dhar for agreeing to be on my committee and for their expert guidance and feedback. I would also like to thank Dr. Peter Rowe and his team including Dr. Lesya Zelenchuk and Dr. Adrian Zelenchuk for the discovery and development of the murikal peptide and their assistance in the murine studies and confocal imaging of the formulation deposition. Lastly, I would like to thank my fellow Forrest lab members and research partners including Dr. Shuang Cai, Dr. Daniel Aires, Dr. Yunqi Zhao, Dr. Sanjeewa Senadheera, Dr. Ti Zhang, Dr. Qiuhong Yang, Peter Kleindl, Abby Petrulis, Jay Jha and Ninad Varkhede. Thank you for your expertise, guidance and friendship.

Table of Contents

1. Introduction

Androgenic alopecia (AGA), commonly known as pattern baldness, is a widespread malady effecting nearly 50% of the Caucasian male and female populations by age 40 and reaching 80% by age 70 in men.[1] Although with reduced prevalence, AGA is also found within other ethnicities. In addition, there is an unmet need for improved treatment of chemotherapy-induced alopecia (CIA) where hair loss occurs in 65% of treatments.[2] While not directly life threatening, the potential psychological effects of hair loss in both male and females is of the utmost concern as patients experiencing hair loss have reported increased stress levels, lower self-esteem, and particularly at younger ages, poor body image perception.[1, 3] Current treatments beyond surgical methods, including topical treatment with minoxidil or finasteride, the active ingredients found in Rogaine® and Propecia® respectively, have shown limited efficacy in restoring hair growth or slowing hair loss.[4] The widespread prevalence of AGA and CIA combined with their associated negative psychological burdens and poorly effective treatment options indicates a dire need for a new and efficient therapeutic to treat these conditions.

In this study, a novel peptide therapeutic, which was observed to increase rates of hair growth in mice when injected intradermally, was formulated into a lipid nanoparticle formulation for efficient topical delivery to the hair follicle and to explore its therapeutic potential to treat AGA, CIA and other hair loss disorders.

2. Background

2.1 Hair growth cycle and follicle biology

Initial hair follicle development and maturation involves a complex network of regulatory signals between the developing dermal mesenchyme and epithelium during gestation, and the details are not yet well understood, specifically those involving initiation. Once the follicle has matured, normal hair growth cycles through defined stages: anagen (growing phase), catagen (regression phase) and a telogen (resting phase). The duration of each stage is dependent on follicle size and location, but under normal conditions 85% of scalp hair is within the anagen phase, lasting on average 2-6 years.[5] The total cycle is controlled by an array of cell signaling molecules and pathways involving cytokines, hormones and neurotransmitters targeting the proliferation of keratinocytes located at the bulb of the hair shaft.[1]

Anatomically, the hair follicle complex is termed the pilosebaceous unit (Figure 1) and is comprised of the hair follicle, sebaceous gland and arrector pili muscle. Located at the base of the hair shaft is the hair bulb, which rests on the dermal papilla. The dermal papilla and the proliferating keratinocytes are supplied nutrients via an underlying capillary.

2.2 Androgenic (AGA) and chemotherapy-induced (CIA) alopecia

Androgens are a general term for compounds, usually steroid hormones such as testosterone, which control development of male associated traits. Although the detailed etiology of AGA is largely unclear, the androgen-dependent nature of the disorder,

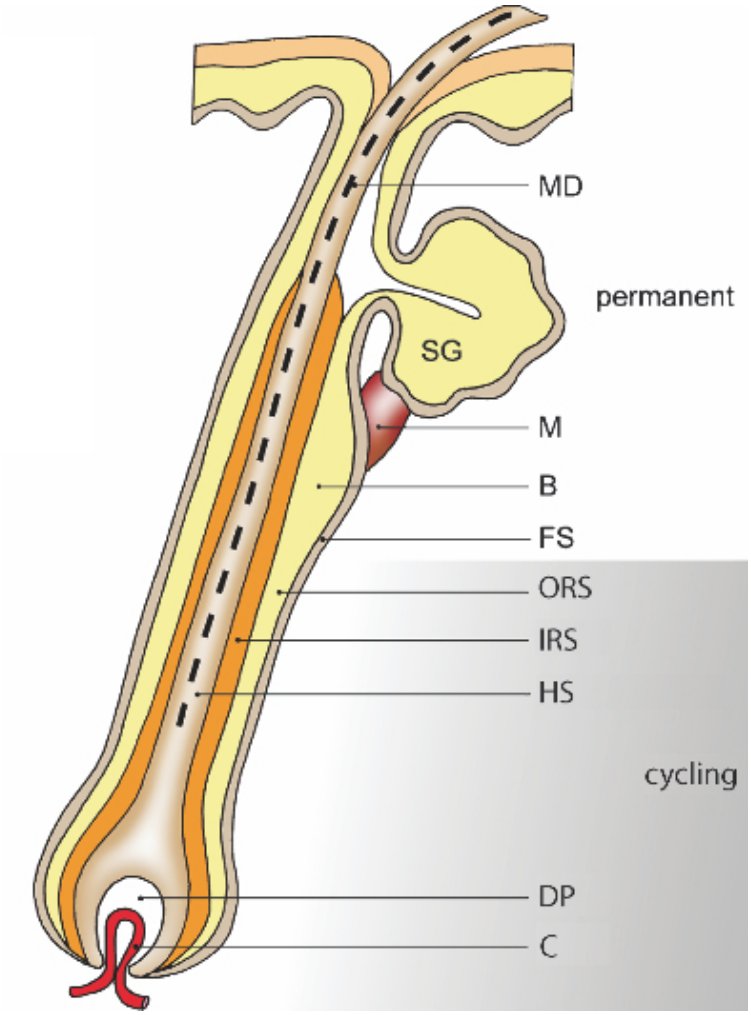

Figure 1. Human pilosebaceous unit. From top: (SG)-sebaceous gland, (M)-arrector pili muscle, (HS)-hair shaft, (DP)-dermal papilla, (C)-capillary. Adapted from Blume-Peytavi, U., Whiting, D. A. & Trüeb, R. M. XXVI, 564 (Springer-Verlag Berlin Heidelberg, 2008).

particularly that of dihydrotestosterone (DHT), is commonly accepted. DHT is the 5α-reduced version of testosterone and has been identified as a key factor in the induction of androgen dependent balding in some patients.[6] Although abnormal DHT and other hair growth signaling molecules indicate a strong potential for the onset of baldness, these abnormalities alone are not solely responsible for development of AGA. In addition, genetically inherited predispositions within 5α-reductase and androgen receptor genes among others as well as age related alterations in androgen controlled mechanisms need to be considered.[1]

CIA, which is also referred to as dystrophic anagen effluvium, is characterized by diffuse hair loss following chemotherapeutic cancerous tumor treatment as a result of the direct toxic effects on rapidly dividing bulb matrix cells found at the dermal papilla. Like AGA, CIA hair loss is first characterized by miniaturization of the follicle leading to thinning and shortening of the hair, prior to entering the telogenic phase where the hair is excluded from the follicle. Fortunately, after cessation of treatment, patients regain near full operation of their pre-treatment anagenic cycle and thus regain hair length and thickness. [1, 2]

2.3 Current treatment options for AGA and CIA

Currently, two main compounds exist for the treatment of AGA associated pattern baldness, minoxidil and finasteride. Minoxidil, the active ingredient found in Rogaine®, has a mostly unclear mechanism of action, but it is believed to activate follicles at later stages in the growth cycle into the androgenic phase through its vasorelaxant effect. A 10-12% increase in target area hair counts is seen with patients using the 5% formulation

with no increase in hair shaft thickness.[1] Minoxidil is currently marketed as a topical solution and a foam-based formulation. The twice daily recommended dose of minoxidil has shown adverse effects including nausea and other systemic associated toxicity including cardiotoxicity and dyspnea.[7]

Unlike minoxidil, finasteride acts to counter alopecia related disorders through inhibition of type 2 5α-reductase, the enzyme required to convert testosterone to DHT. Daily oral doses (1 mg) have shown efficacy in slowing baldness and 66% of patients have reported improved hair growth after about 12 months of treatment.[8] Although treatment with finasteride has not been shown to regrow lost hair, inhibition and reversal of follicle miniaturization associated with androgenic alopecia has been observed. Adverse effects of oral dosage forms of finasteride mainly include an increased risk of sexual dysfunction.[9, 10]

In regard to the treatment of CIA, preventative minoxidil treatment of patients undergoing early stages of chemotherapy showed limited capacity to prevent hair loss when compared to placebo.[2, 11] Specific trials on the effect of finasteride to prevent chemotherapy-induced alopecia were not found.

2.4 Murikal (SPR4-peptide) promotes Wnt/β-catenin pathway and subsequent hair growth

SPR4 or murikal is a recently described 4.2-kDa synthetic PHEX-peptide observed to bind and neutralize ASARM-peptides in addition to its positive effects on bone development (Sequence in Figure 2). Much of murikal's positive effects can be contributed to its inhibition of sclerostin (SOST).[12-17] Of interest to this application,

sclerostin is a known inhibitor of the Wnt β-catenin canonical pathway, which is a prominent signaling pathway for both early hair follicle formation[18] as well as the induction of new hair growth cycles.[1] The proposed mechanism of action is depicted in Figure 2. Proof of concept for murikal as a potential hair growth therapeutic was further demonstrated following daily intradermal injections of the peptide for 11 days (Figure 3). The mice shown in Figure 3 were of wild-type (C57BL/6) with complete depilation of their dorsal hair with Wax Strips (Del Laboratories,Farmingdale, NY) prior to the peptide treatment.

2.5 Lipid nanoparticles for improved topical delivery of macromolecules

In response to the encouraging results seen after daily intradermal injections of murikal in mice to induce increased hair growth rates, a topical approach was explored to remove the need for injections and provide a more efficient and possible more effective targeted therapy to the follicle structure.

Lipid nanoparticles and particularly liposomes have been used for a wide range of drug delivery applications and compounds. A liposomal formulation is a promising delivery method for this application in that a wide variety of compounds may be encapsulated in the amphipathic particles, they may provide additional chemical stability to the peptide, liposomes induce little to no off-site toxicity, and most importantly, liposomes may be tuned to fit a wide variety of physicochemical environments providing a carrier with compatible properties to the highly lipophilic environment at the outer surfaces of the skin and pilosebaceous unit.[19]

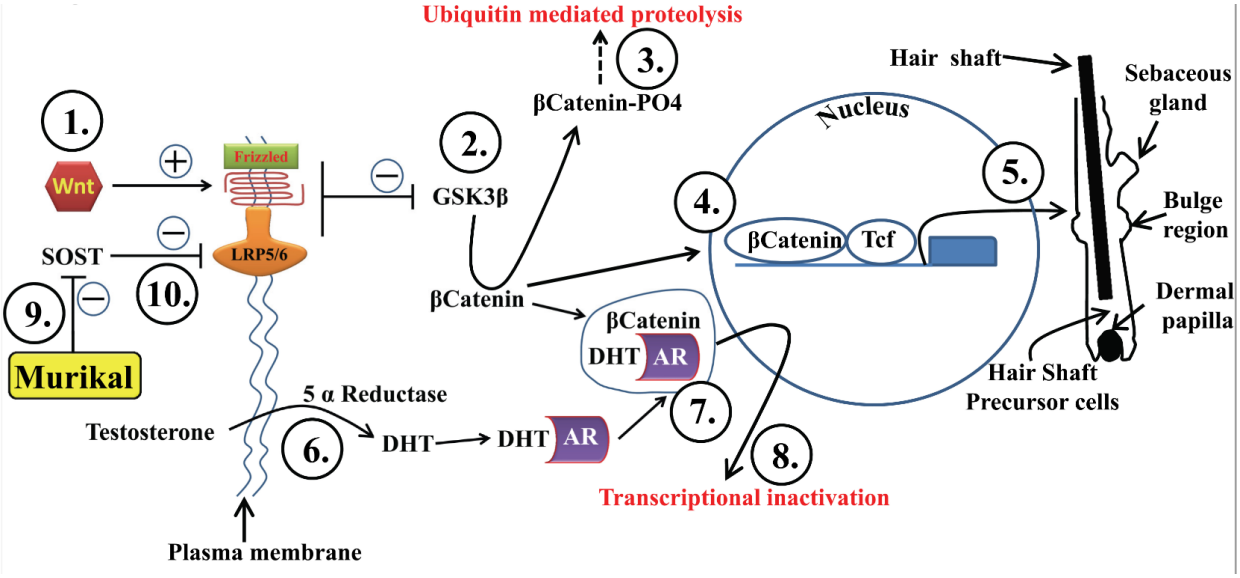

Murikal (SPR4) Sequence: H-TVNAFYSASTNYPRSLSYGAIGVIVGHEFTHGFDNNGRGENIADNG-OH

Figure 2. Proposed mechanism of murikal on increasing hair growth rate. Murikal inhibition of sclerostin (SOST) (9) and its downstream blockade (10) of Wnt and its association with the FRZ/LRP5/6 receptor complex (1). Activation of this complex leads to inhibition of GSK3β (2), which is responsible for the removal of cytoplasmic β-catenin through ubiquitin mediated proteolysis following phosphorylation (3). Higher levels of cytoplasmic β-catenin reduces the negative effects of DHT deactivation of β-catenin following the reduction of testosterone via excess 5-α reductase (6) and binding with androgen receptors (7 & 8). Overall leading to increased nuclear translocation of β-catenin (4) and increased transcription of factors signaling hair growth (5). Diagram developed by Dr. Peter Rowe and reproduced with permission.

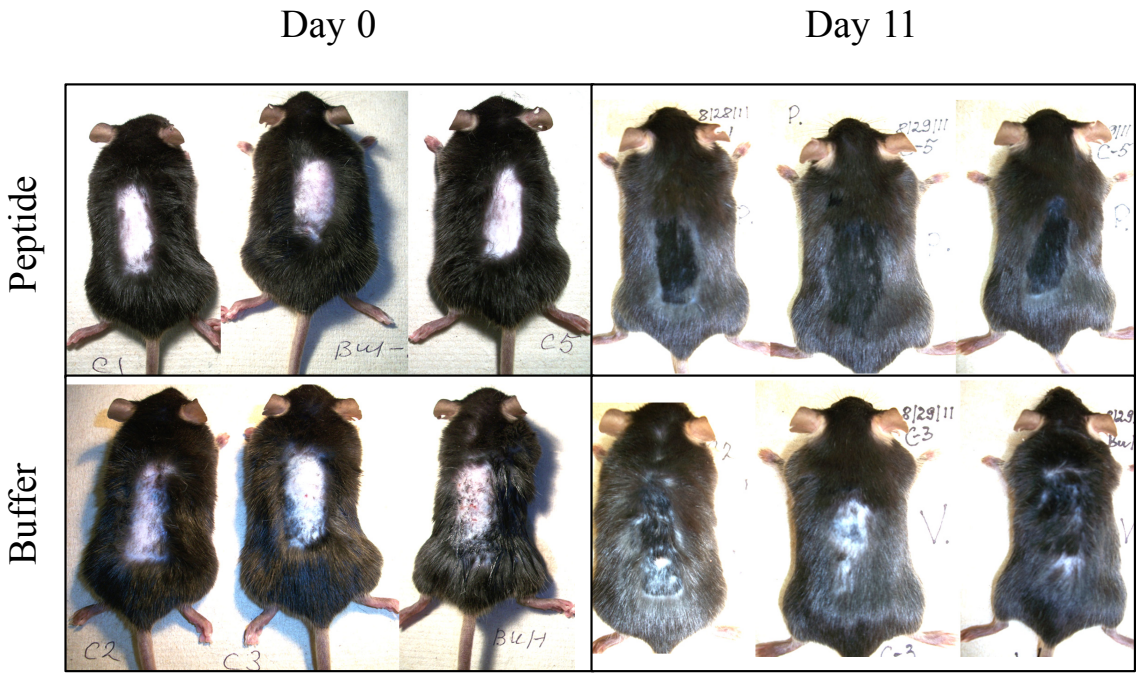

Figure 3. Wild type mice (C57BL/6) at Day 0 with treatment area hair removed with complete depilation and at Day 11 following daily intradermal injections of murikal (SPR4-peptide) or buffer control. Results obtained by Dr. Peter Rowe and reproduced with permission.

Many different active drugs, both small and large molecule, have been targeted to hair follicles with liposomal carriers of various compositions. Pairing a liposomal formulation to an active ingredient (API) is a balance of matching physicochemical properties to yield high and efficient encapsulation of the API, while also yielding particle biophysical properties that give optimum deposition into the targeted environment of the follicle. Successful liposomal delivery of drugs to follicles includes non-ionic[20-22], cationic[23, 24] and anionic[25-27] formulations developed by various manufacturing methods.[7, 28-31]

In this study, murikal was initially formulated into a phosphatidylcholine (PC) based liposomal formulation and delivered topically to mice to show both qualitatively, via confocal microscopy imaging, and quantitatively, via pixilation of hair growth, the peptide's potential as a topically delivered therapeutic. Once shown to be successful, formulations of various compositions were gathered from successful literature attempts and similarly tested by confocal microscopy for optimal performance. Two lead formulations were chosen from this study and subjected to a 30-day stability study of particle stability, drug release and drug degradation. These two lead formulations were finally applied *ex-vivo* to human donor facial tissue to determine deposition translatability to human follicles.

3. Experimental

3.1 Materials

L-α-Phosphatidylcholine (PC) from dried egg yolk, Type X-E, >=40% (enzymatic), Cholesterol (CH), 95%, α-Tocopherol (α-Toco), 96%, Dilaurin Mixed Isomers (GDL, Glyceryl dilaurate), Brij S10 (Polyethylene glycol octadecyl ether, Polyoxyethylene (10) stearyl ether) (POE-10), and Phytonadione, Vitamin K_1 were purchased from Sigma-Aldrich Co (St. Louis, MO, USA). 1,2-dioleoyl-3-trimethylammonium-propane (DOTAP) (chloride salt) was purchased from Avanti Polar Lipids (Alabaster, AL, USA). Murikal (SPR4-peptide), 80%, and Biotinylated-murikal were synthesized by PolyPeptide Laboratories (San Diego, CA, USA), sequence in Figure 2. Double distilled water (ddH_2O) was used in the syntheses and characterization of the lipid particles. Tris Base and Sodium chloride were purchased from Fisher Scientific (Pittsburgh, PA, USA). Ethanol, 200 Proof, was obtained from Decon Laboratories, Inc.. All other solvents were of HPLC grade and obtained from Fisher Scientific. Table 1 outlines all liposomal formulations used and their adapted sources.

Men's Rogaine® Extra Strength, 5% Minoxidil Topical Solution, Unscented was purchased from a local pharmacy.

Alexa Fluor 594 (red) #S32356 and 488 (green) #S32354 were purchased from Molecular Probes (USA). DyLight™ 488 (A_{max} 493 nm, #53024) and Fluorescein isothiocyanate (FITC) antibody labeling kits were purchased from Thermo Scientific; Pierce Biotechnology (Rockford, Il 61105 USA).

Form. #	Composition*	Weight Ratio	Lipid Concentration, (mg/mL)	Ethanol Concentration, % (v/v)
1	PC;EtOH[28]	100	103.8	4.3%
2	PC/CH/DOTAP/α-Toco;$CHCl_3$/MeOH[20, 21, 30, 32]	68.4/21.1/9.6/ 0.9	50	0%
3	PC/CH/DOTAP/ α-Toco;EtOH[20, 21, 30, 32]	68.4/21.1/9.6/ 0.9	50	4.3%
4	GDL/CH/ POE-10/DOTAP/ α-Toco;EtOH[20, 21, 32]	50/14/23/12/1	50	0%
5	GDL/CH/POE-10/DOTAP/ α-Toco;EtOH[20, 21, 32]	50/14/23/12/1	50	4.3%
* α-Tocopherol (α-Toco) replaced with Phytonadione, Vitamin K_1, prior to *ex-vivo* human tissue trials due to reports of toxicity.				

Table 1. Liposomal formulations screened for optimum delivery of murikal to follicle

3.2 Methods

3.2.1 Preparation of murikal encapsulated liposomes

Egg phosphatidylcholine liposome formulation (F,1) was made by a modified ethanol injection method described elsewhere.[28] Briefly, L-α-Phosphatidylcholine (2.39 g/mL) was dissolved in ethanol. The solution was vortexed for 5 minutes and sonicated for 10 minutes or until a clear solution was achieved. Subsequently, murikal, biotinylated-murikal or fluorescently labeled-murikal (5 mg/mL) was dissolved in 25 mM Acetic acid at 1mg/100ul. Once dissolved, 50 mM Tris pH 7.4/150 mM NaCl was added drop wise to a peptide concentration of 5mg/mL The murikal solution was added drop wise (1.5 mL/h) to the lipid ethanolic solution using a syringe pump while constantly stirring. Then additional 50 mM Tris pH 7.4/150 mM NaCl (3.8X to murikal solution volume) was added drop wise (1.5 mL/h) using a syringe pump while constantly stirring. The final solution was stored at 4°C and covered from light exposure. The final formulation contained 103.8 mg/mL of lipid, 4.3% (v/v) of ethanol, and 0.99 mg/mL of murikal. Ethanol at up to 4.3% (v/v) was used within the formulation as a penetration enhancer, above this level would potentially cause unwanted irritation or redness when applied.

Formulations 2-5 (F,2-5) in Table 1 were prepared similarly to the PC liposome protocol above with slight modifications. All formulations were prepared using variations of the ethanol injection method due to its simplicity and verified efficacy from the first generation formula. The following example applies to (F,2-5) with specified lipids and solvent systems seen in Table 1. For F,3, L-α-Phosphatidylcholine/Cholesterol/1,2-dioleoyl-3-trimethylammonium-propane (DOTAP)/ α-Tocopherol were dissolved in

ethanol to 125 mg/ml with a molar ratio of 55.7:34.3:8.6:1.3, PC:CH:DOTAP: α-Tocopherol. The solution was vortexed for 5 minutes and sonicated for 10 minutes or until a clear solution was achieved. Murikal (1.73 mg/mL) was dissolved in 25 mM acetic acid with subsequent addition of 50 mM Tris pH 7.4/150 mM NaCl, pH 7.4 (1:9, AcOH:Tris). The lipid ethanolic mixture was heated to 60°C for 2-3 min and the SPR4 solution heated to 37°C for 2-3 min. The murikal solution was added drop wise to the lipid while constantly stirring until a 2:3 solvent-to-buffer ratio was achieved. Subsequently, organic solvents were removed by rotoevaporation entirely or to 4.3 % (v/v) (Organic solvent content of each formulation can be found in Table 1). Solvent removal continued until all foaming within the mixture ceased. The final solution was stored at 4°C and covered from light exposure. The final formulation contained 50 mg/mL of lipid, 0% (v/v) or 4.3% (v/v) of ethanol and 0.99 mg/mL of murikal.

3.2.2 Quantification of murikal encapsulated in liposomal formulation

The amount of murikal incorporated into any of the liposomal formulations was quantified by the following method. A known volume of the final liposome solution was disrupted by a 10X dilution using dimethyl sulfoxide (DMSO) to determine total peptide content. A second vial of the same initial volume of the liposome solution was centrifuged at 13,300Xg for 15 min. The supernatant, unencapsulated murikal, was removed and placed in a new centrifuge cuvette and the pellet, encapsulated murikal, was retained. This procedure was repeated twice or until a pellet was no longer visible after centrifugation. The pellets were then combined and dissolved into enough dimethyl sulfoxide (DMSO) to match the volume of the total peptide vial. Both vials, total peptide

and encapsulated peptide, were subjected to 2 minutes of vortex mixing and 10 minutes of sonication. The concentration of murikal was determined in each by gradient RP-HPLC against a known standard concentration profile. The HPLC system consisted of a Shimadzu LC-2010CHT (Shimadzu Scientific Instruments, Inc., Columbia, MA, USA) with in-line deuterium lamp ultraviolet detector. A Supelco Discovery HS C18 analytical column (150 × 4.6 mm; 3 μm) was used for the analysis. The mobile phase consisted of A (ddH_2O, 0.1% formic acid) and B (acetonitrile, 0.1% formic acid), and the linear gradient was 10-100% B over 10 min at a flow rate of 0.8 mL/min. UV absorption was measured at 275 nm. The encapsulation efficiency (EE %) of murikal encapsulated into the liposome particle were calculated using the equation:

EE % = (Corrected AUC of encapsulated (pellet) murikal/Corrected AUC of total murikal) × 100%

3.2.3 Particle size and zeta-potential measurements

The hydrodynamic diameter of the liposomes was measured by dynamic light scattering (DLS) on a ZetaPALS (Brookhaven Instruments Corp., Holtsville, NY) following a 20X dilution in ddH_2O, with stability analysis measurements of lead formulations repeated three times. Zeta potential of liposomes diluted 20X in ddH_2O were measured on a ZetaPALS (Brookhaven Instruments Corp., Holtsville, NY), with stability analysis measurements of lead formulations repeated three times.

3.2.4 Peptide mass spectrometry analysis

Mass spectrometry analysis was performed in conjunction with the KU Mass Spectrometry and Analytical Proteomics Laboratory using a Waters ACQUITY UPLC System coupled with a Thermo Finnigan ESI LQ-FTICR hybrid mass spectrometer. The RP-HPLC method used an Atlantis dC18 Column, 100Å, 3 µm (Waters Inc. P/N 186001279), 5 cm, I.D. 1 mm with gradient elution of mobile phase consisting of A (ddH_2O, 0.1% Formic acid) and B (9:1, Isopropanol:Acetonitrile, 10 mM Ammonium Formate, 0.1% Formic acid), with 1-50% B over 17 min and 50-95% over 2 min at 45-60 µL/min .

3.2.5 Murine *ex-vivo* peptide follicle penetration analysis

All experimental procedures were approved by the University of Kansas Medical Center, Institutional Animal Care and Use Committee (IACUC). Wild type mice (C57BL/6) were treated with liposomal solutions of a particular formulation following complete depilation of dorsal hair by Wax Strips (Del Laboratories,Farmingdale, NY) inducing premature anagen phase of the hair growth cycle. In the first trial using the first generation formulation (F,1), 50 µl of murikal labeled with DyLight™ 488 at 1 mg/ml was applied topically to the depilated region and allowed to absorb for 30 minutes prior to sacrifice. In the second trial where formulations were compared for optimum dermal penetration and follicle localization, 100 µl of biotinylated-murikal at 1mg/ml was applied topically to the depilated region and allowed to absorb for 10 minutes prior to sacrifice. In addition, tissue treated with a DermaRoller microneedle and subsequent aqueous peptide solutions (1mg/mL) were used to compare the follicular penetration

effectiveness of the liposomal formulation. Empty, no peptide, liposomes were used as a control. The treatment area was excised, and paraffin sections of 10% neutral buffered formalin (4% formaldehyde in phosphate buffered saline) fixed skin were prepared for histology and flash frozen in OCT and liquid nitrogen. Cryomolds were cryosectioned and stained with DAPI-Progold to visualize the nuclei of the cells. At this point, if biotinylated-murikal was initially applied, Alexa Fluor 488 or 594 streptavidin conjugates were also applied to the cryosectioned slides for peptide imaging.

3.2.6 Murine *in-vivo* hair growth rate acceleration assessment

Anagen hair growth was induced on the dorsal surface of 5-week old wild type (C57BL/6) mice by wax strip treatment prior to application of the peptide formulations. Mice were treated with daily (50 μl) applications of murikal (1mg/ml) liposomal formulation, allowing 10 minutes for absorption. Similarly, minoxidil was applied daily at the manufacturer's recommended doses. Empty, no peptide, liposome vehicles were applied at equal volumes and intervals to control treatment groups. Contrast images of hair growth were analyzed using a pixel conversion program, GelQuant.Net (BiochemicalLabSolutions.com).

3.2.7 Lead formulations stability study

Two lead formulations were selected following analysis of murine follicle penetration of all formulations found in Table 1. Triplicate batches of each lead formulation were produced. Measurements of encapsulation efficiency of each batch were made on Day 0, 1, 2, 7, 14 and 28. Particle size and zeta potential of each batch

were measured on Day 0, 1, 9, 22, and 34. Results are expressed as average measurements with standard deviation.

3.2.8 Human *ex-vivo* peptide follicle penetration analysis

All experimental procedures were approved by the University of Kansas Medical Center, Institutional Review Board (Human Subjects Committee). Human donor scalp tissue following cosmetic surgery was treated with (10µl) of murikal (1mg/ml) liposome formulation spiked with 3.5 % (m/m) FITC-labeled peptide. Following 15 minutes or 30 minutes of absorption time, 6 mm biopsy punches of the skin were made and flash frozen in OCT and liquid nitrogen. Cryomolds were cryosectioned and imaged by confocal microscopy as described previously. 50 mM Tris pH 7.4/150 mM NaCl was used as a control.

4. Results

4.1 Proof of concept: Liposomal topical therapeutic efficacy

4.1.1 Murine *ex-vivo* peptide follicle penetration analysis

DyLight™ 488 conjugated murikal was successfully encapsulated within a first generation egg phosphatidylcholine liposome formulation (F,1) at a concentration of 1 mg/mL with an encapsulation efficiency of 71% (m/m) measured by RP-HPLC. Significant dermal penetration and follicular localization was observed by confocal analysis of treated tissue (Figure 4). Co-imaging of nuclei (DAPI-blue) and murikal (DyLight™ 488-green) 30 minutes after applying the formulation, indicate regions of specific cellular uptake of the peptide at deep portions of both the dermis and follicle as well as uptake within deep dermal neuronal cells (pacinian corpuscle). Buffer-only murikal solutions without lipid addition at 1mg/ml peptide were applied to the depilated dorsal skin of the mice, but sufficient peptide did not absorb for detection by confocal imaging.

4.1.2 Murine *in-vivo* hair growth rate acceleration assessment

Daily application of F,1 with murikal at a concentration of 1 mg/mL and an encapsulation efficiency of 71% (m/m) resulted in quantifiably significant improvements in hair growth rate in wild type mice (C57BL/6) when compared to minoxidil and empty (no peptide) liposomal treatments (Figure 5). Digital quantification of contrast images of the treated areas (Figure 6) shows significant and major increases in the hair growth rate of mice treated with daily 50 µl topical application of the peptide liposome formulation versus both minoxidil and empty liposomal vehicles.

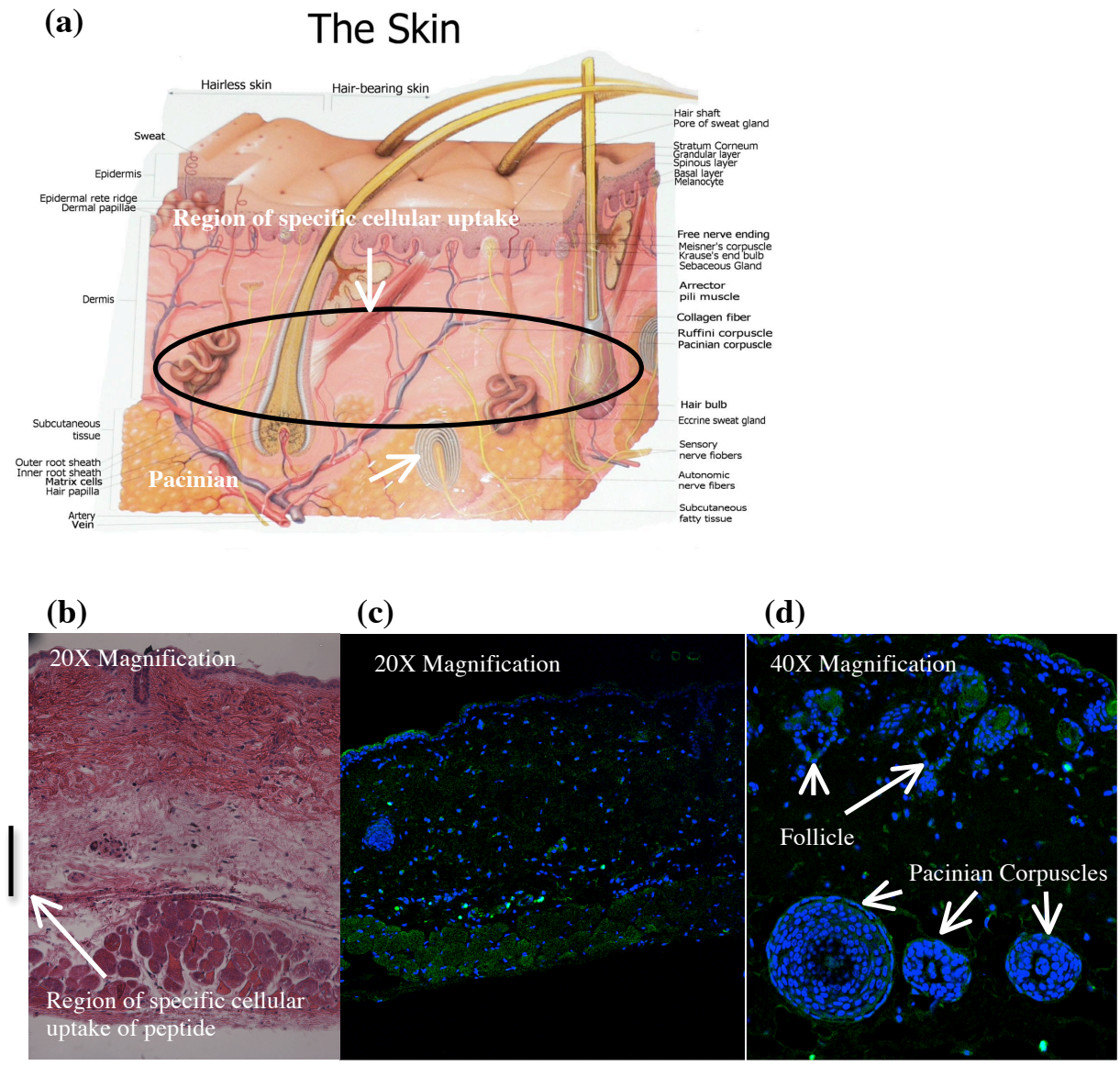

Figure 4. Confocal microscopy analysis of the dermal penetration of F,1. (a) Cross sectional diagram of skin with region of peptide specific cellular uptake and pacinian corpuscles noted, (b) histological cross section at 20X magnification and region of peptide specific cellular uptake noted, (c) 20X magnification confocal microscopy image of cryosectioned tissue treated with F,1, cells indicated by blue DAPI nuclear stain and DyLight™ 488-Murikal indicated in green, (d) 40X magnification confocal microscopy image with follicle and pacinian corpuscle structures noted.

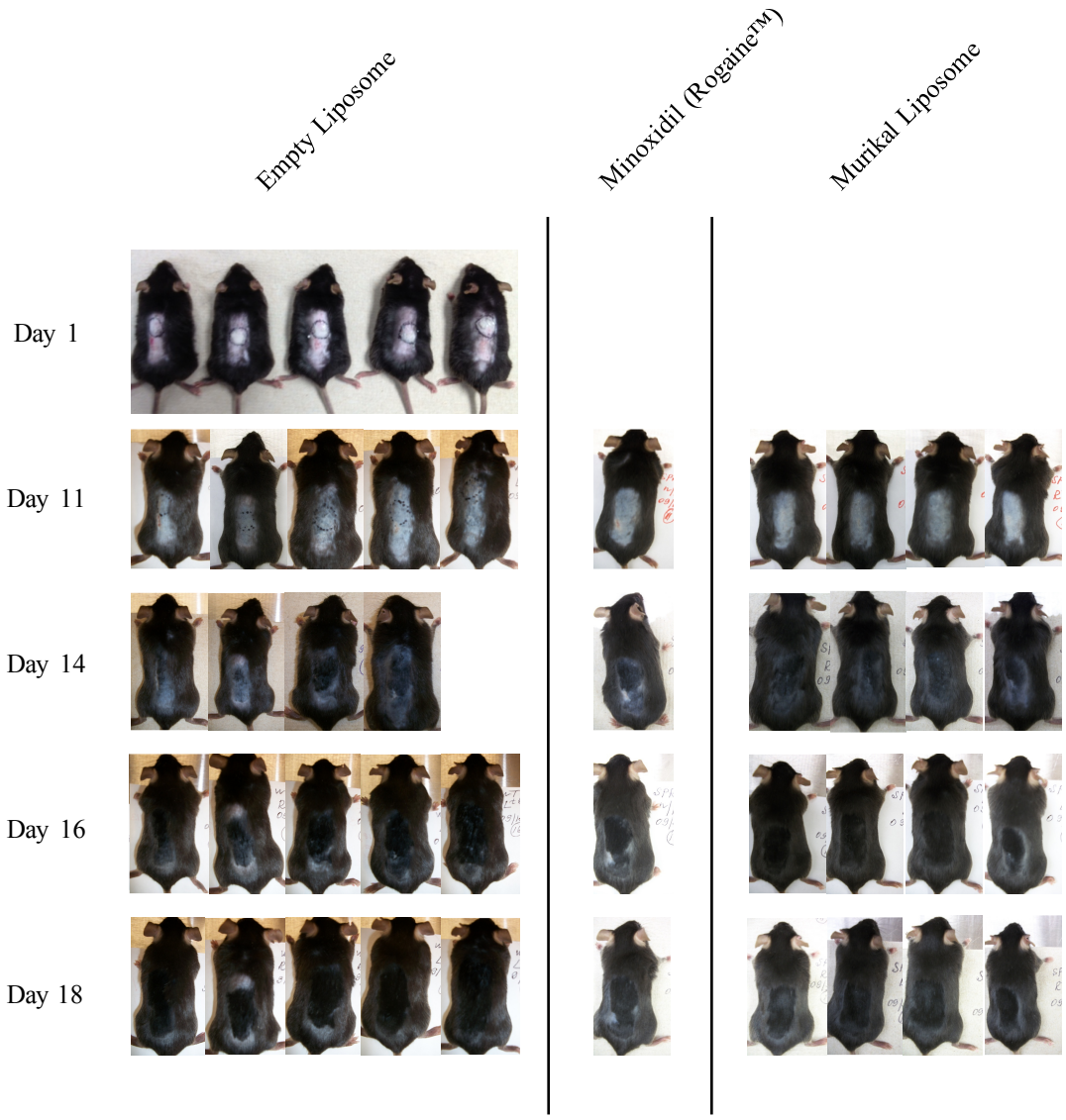

Figure 5. Accelerated hair growth seen in wild type mice treated with daily liposome formulations of murikal (50 µl) compared to minoxidil (Rogaine®) and empty (no peptide) liposome formulations. Anagen phase induced by complete depilation of dorsal hair at Day 0.

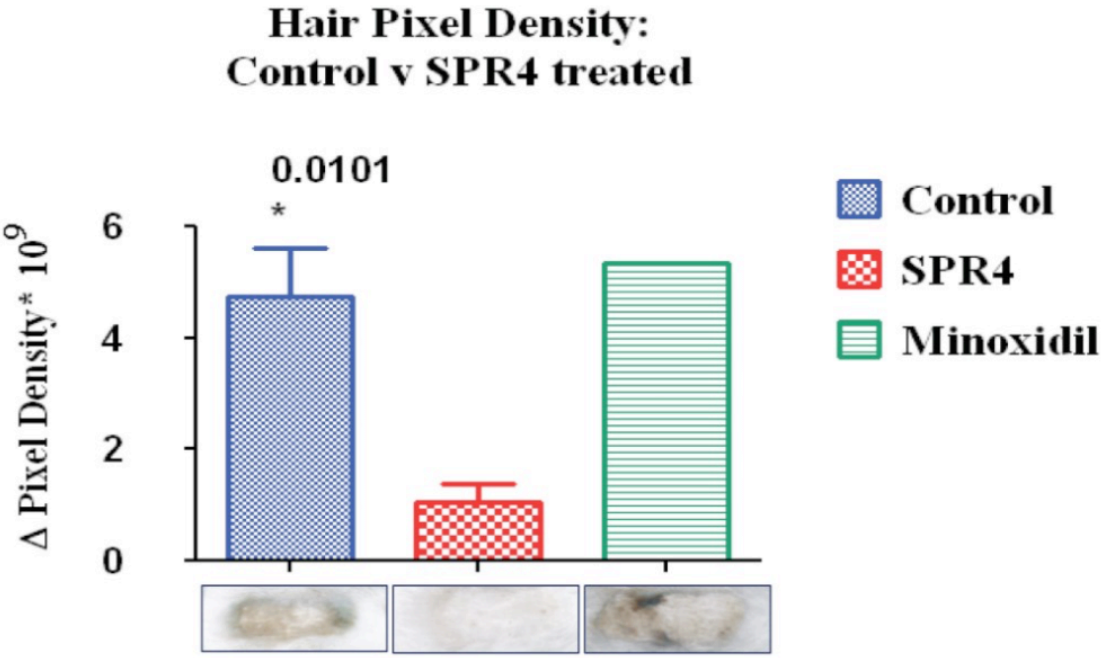

	Control	SPR4	Minoxidil
Mean	4.759	1.046	5.352
Std. Deviation	2.105	0.6964	0.0
Std. Error	0.8592	0.3482	0.0

Figure 6. Quantitative analysis of wild type mice at Day 14 of daily liposomal formulations of murikal following complete depilation of treatment area indicates significant and major increases in growth rate when compared to minoxidil and empty (no peptide) liposome control. Note, the lower the change in pixel density the greater the hair density.

4.2 Formulation optimization and *ex-vivo* murine screening

Four additional formulations as listed in Table 1 were adapted from the sources cited and applied topically to the depilated dorsal skin of wild type mice to assess their follicular penetration compared to F,1. All formulations when applied appeared visually as a milky white emulsion with viscosity near water. The encapsulation efficiency, size and zeta potential of each formulation are listed in Table 2. Confocal analysis indicated enhanced dermal penetration and follicular localization with F,3 and F,4 as compared to all other formulations used (Figure 7). Murikal dissolved in an aqueous buffer (no liposomes) and applied to depilated skin treated with a microneedle roller showed no significant dermal penetration or follicle localization.

4.3 Lead formulations particle and peptide stability

F,3 and F,4 were advanced as lead formulations into a time and temperature dependent stability study, analyzing both the colloidal and chemical stability of the liposomes and peptide.

Encapsulation efficiency was monitored by centrifugal phase separation and subsequent peptide resolution by RP-HPLC. F,3 liposomal particles had an encapsulation efficiency of 83.73 ± 9.62 % (m/m) at Day 0, 86.66 ± 6.65 % after 28 days stored at 4°C, 119.68 ± 20.55 % after 28 days stored at 25°C. F,4 liposomal particles had an encapsulation efficiency of 65.15 ± 22.80 % at Day 0, 104.05 ± 18.08 % after 28 days stored at 4°C, 95.72 ± 1.29 % after 28 days stored at 25°C (Figure 8).

F,3 and F,4 liposomal particle sizes and zeta potential were monitored by dynamic light scattering and phase analysis light scattering of diluted samples with results shown

in Figure 9, 10, 11 and 12. F,3 liposomal particles had an effective diameter of 287 ± 18 nm at Day 0, 328 ± 37 nm after 34 days stored at 4°C, 320 ± 48 nm after 35 days stored at 25°C. F,4 liposomal particles had an effective diameter of 2231 ± 1104 nm at Day 0, 9180 ± 5947 nm after 35 days stored at 4°C, 17524 ± 11736 nm after 35 days stored at 25°C. F,3 liposomal particles had a zeta potential of 74.25 ± 10.03 mV at Day 0, 74.94 ± 11.27 mV after 34 days stored at 4°C, 81.03 ± 8.12 mV after 35 days stored at 25°C. F,4 liposomal particles had a zeta potential of 4.08 ± 6.85 mV at Day 0, 66.97 ± 1.85 mV after 34 days stored at 4°C, -2.45 ± 9.28 mV after 35 days stored at 25°C.

Peptide stability was monitored using a Thermo Finnigan ESI LQ-FTICR hybrid mass spectrometer. Lyophilized murikal dissolved in 25 mM Acetic acid at 1mg/100ul and then diluted to 1mg/ml with 50 mM Tris pH 7.4/150 mM NaCl and immediately analyzed supported the manufacturer's certificate of analysis spectrum with major species corresponding to peptide charge states at $(M+3H)^{3+}/3$= 1631.1, $(M+4H)^{4+}/4$= 1223.6, $(M+5H)^{5+}/5$= 979.1 (Figure 13). After 40 days stored at 4°C and 25°C, F,3 and F,4 were diluted 5X in 200 proof ethanol and analyzed again for peptide mass. All major charge states as stated above in the parent peptide were within the spectra of the peptide associated peak at a t_R=11 min (Figure 14). Similarly, major charged states of the parent peptide were seen within the spectra of both F,4 formulations stored at the two temperatures for one month (Figure 15). Unlike F,3, a co-eluting detergent is seen in the spectra of F,4, with a peak pattern at 500-1000 m/z in both conditions. This spectra is likely associated with the Dilaurin mixed isomers or polyethylene glycol octadecyl ether surfactants not found in F,3. Both sets of spectra at 25°C have an apparent lack in TIC of the parent peptide when compared to their 4°C counterpart.

4.4 Human *ex-vivo* peptide follicle penetration analysis

F,3 and F,4 with fluor-labeled murikal were applied to excised human facial tissue for 15 and 30 minutes and then flash frozen for confocal imaging. Confocal images of tissue treated with both formulations for 30 minutes in Figure 16 shows no significant dermal penetration or follicle localization of the fluor-murikal nor a general presence of unpenetrated murikal at the tissue surface.

Form. #	Composition*	EE, % (m/m)	Effective Diameter, nm**	Polydispersity**	Zeta Potential, mV**
1	PC;EtOH	52.5 %	731 ± 16	0.31 ± 0.03	-0.93 ± 8.15
2	PC/CH/DOTAP/ α-Toco;$CHCl_3$/MeOH	82.4 %	40,335 ± 11,390	0.66 ± 0.30	78.99 ± 8.05
3	PC/CH/DOTAP/ α-Toco;EtOH	83.7 %	287 ± 18	0.29 ± 0.03	74.25 ± 10.03
4	GDL/CH/ POE-10/DOTAP/ α-Toco;EtOH	65.1 %	2,231 ± 1,104	0.41 ± 0.06	4.08 ± 6.85
5	GDL/CH/POE-10/DOTAP/ α-Toco;EtOH	84.1 %	1,667 ± 161	0.38 ± 0.04	4.74 ± 5.19

* α-Tocopherol (α-Toco) replaced with Phytonadione, Vitamin K_1, prior to *ex-vivo* human tissue trials due to reports of toxicity.
**Plus/minus indicate standard deviation from mean

Table 2. Physical characterization of screened formulations to determine optimum dermal penetration and follicle localization of murikal peptide.

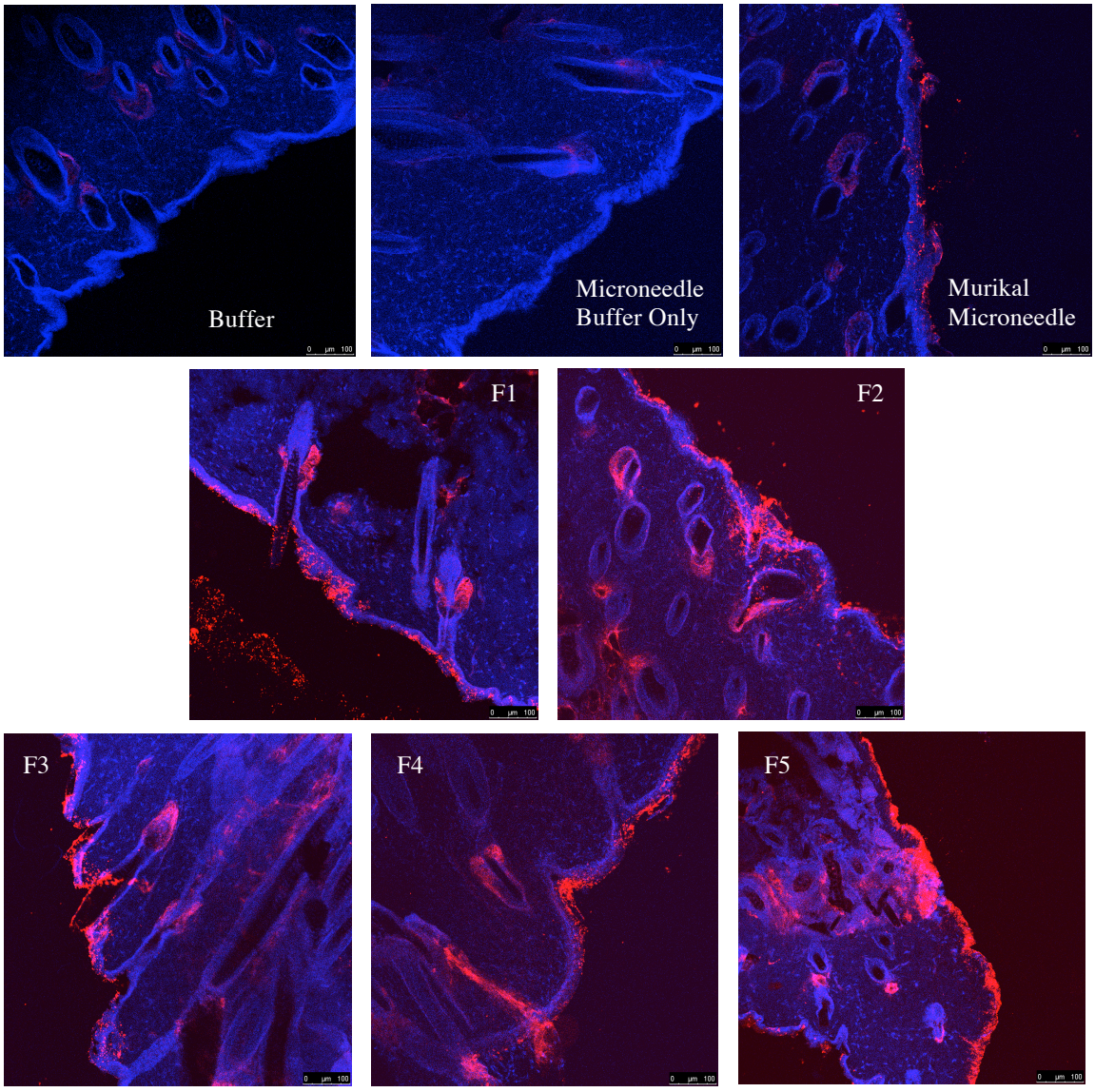

Figure 7. Confocal analysis of cryosectioned murine tissue treated with an array of formulations to optimize the dermal penetration and follicle localization of murikal. F,3 and F,4 taken as lead candidates.

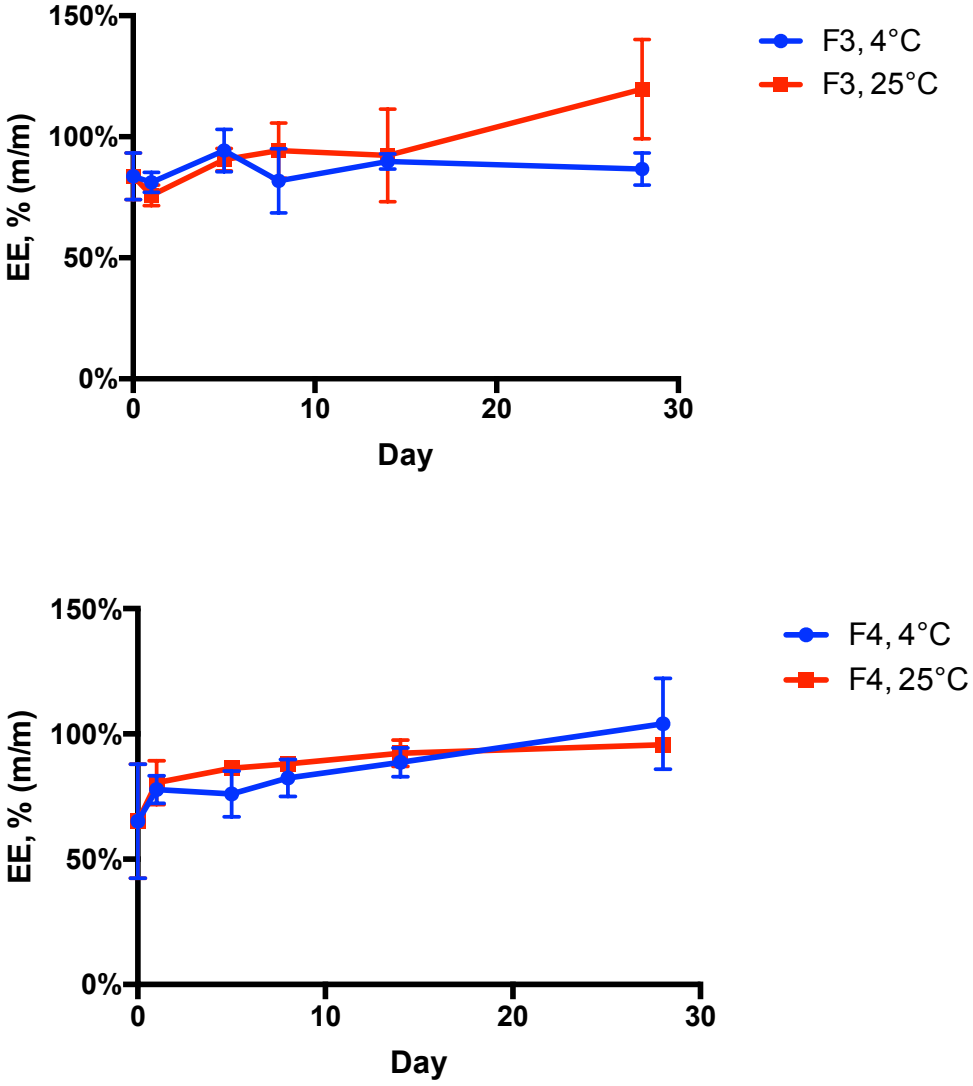

Figure 8. F,3 and F,4 liposome stored at 4°C and 25°C with peptide encapsulation efficiency % (EE %) measured at intervals for one month. Error bars indicate standard deviation from the mean.

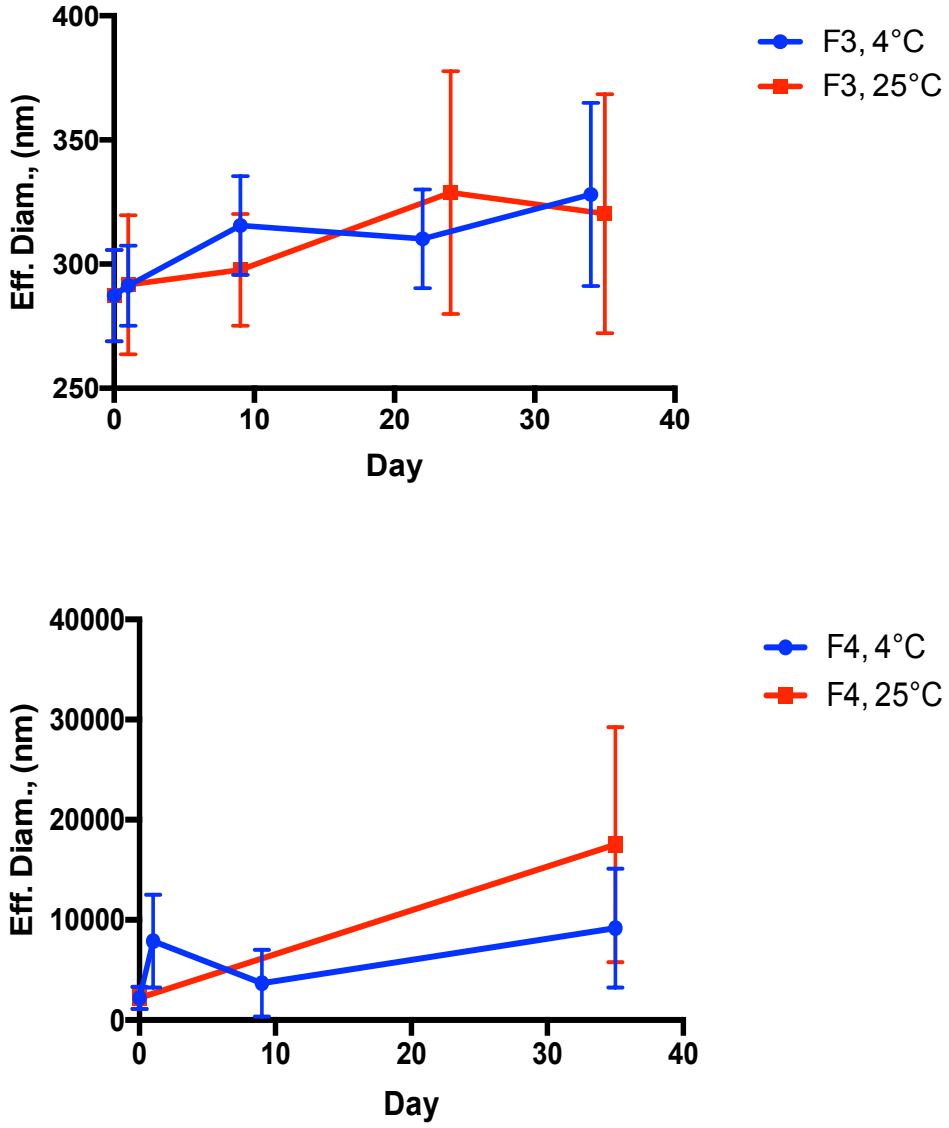

Figure 9. F,3 and F,4 liposome stored at 4°C and 25°C with effective diameter measured at intervals for one month. Error bars indicate standard deviation from the mean.

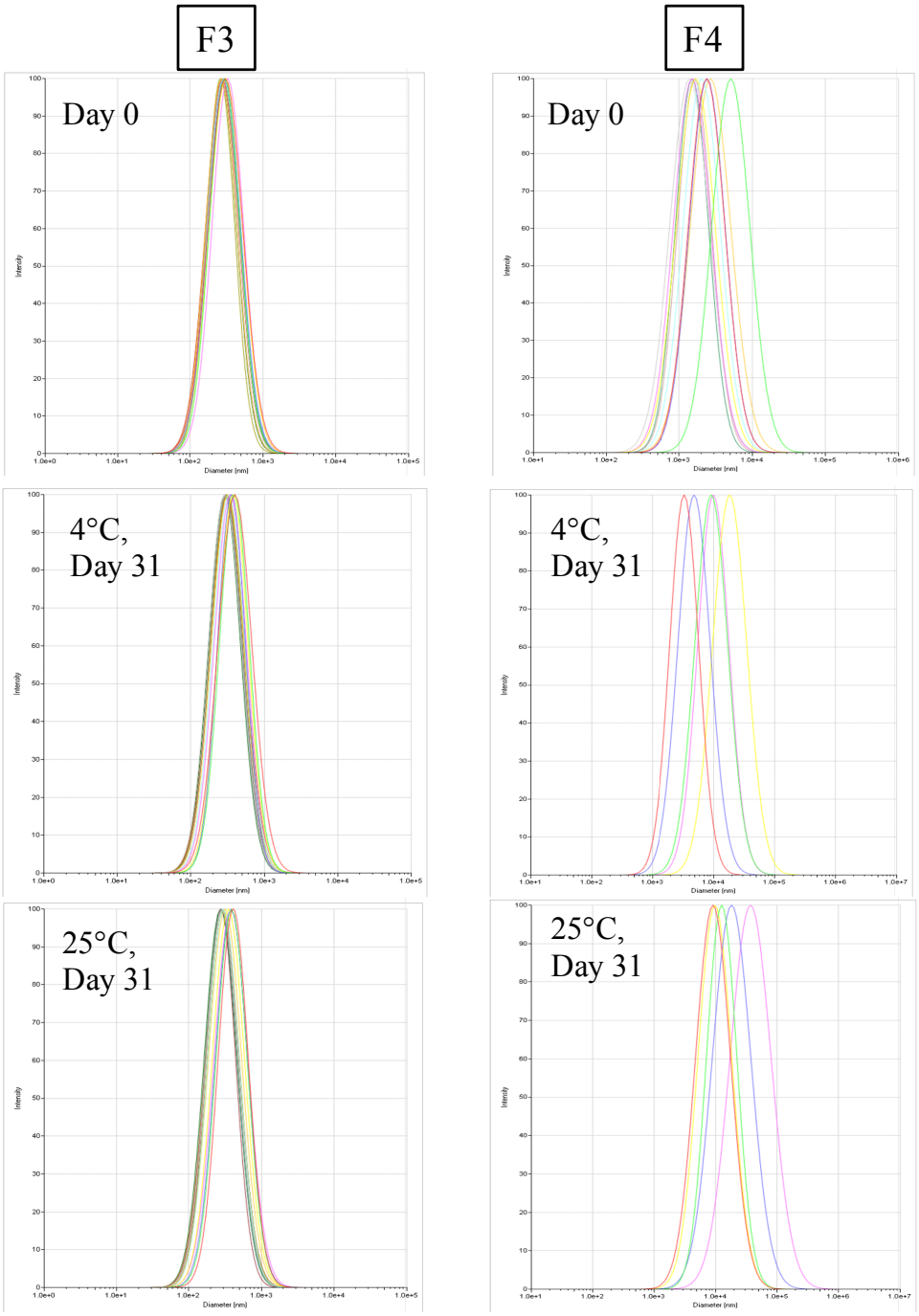

Figure 10. Logonormal distributions of F,3 and F,4 effective diameters at Day 0 and after one month stored at 4°C and 25°C. Each set represents data from all batches analyzed at each condition.

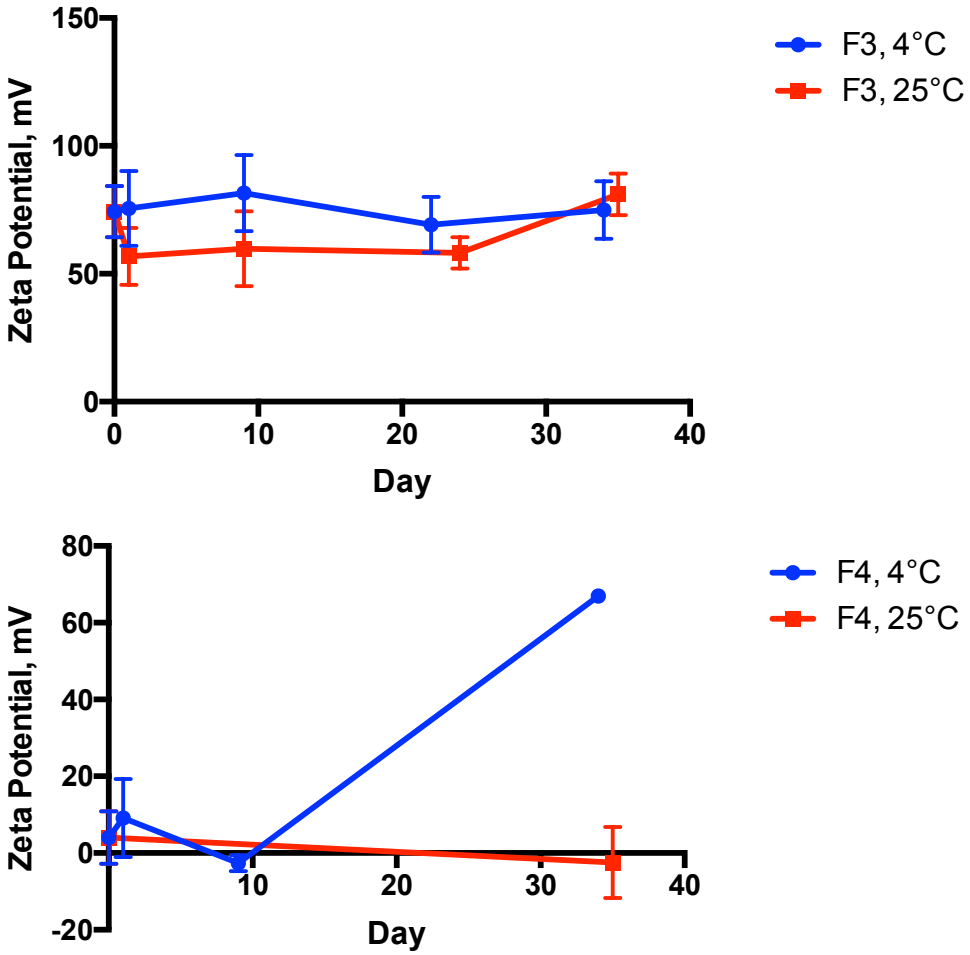

Figure 11. F,3 and F,4 liposome stored at 4°C and 25°C with zeta potential measured in intervals over one month. Error bars indicated standard deviation from the mean.

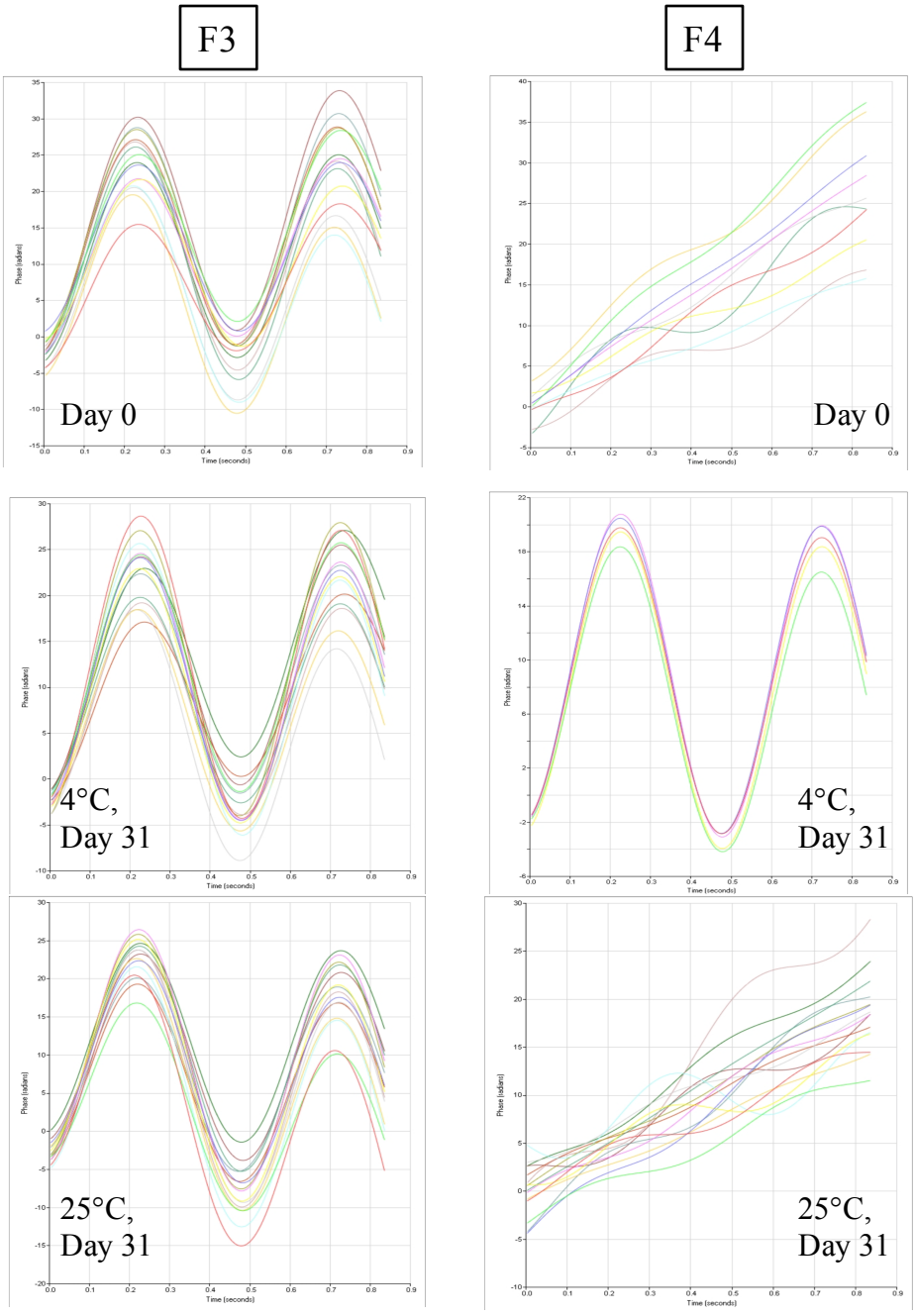

Figure 12. Phase analysis light scattering (PALS) results from F,3 and F,4 stored at 4°C and 25°C and measured for zeta potential at specific intervals over one month.

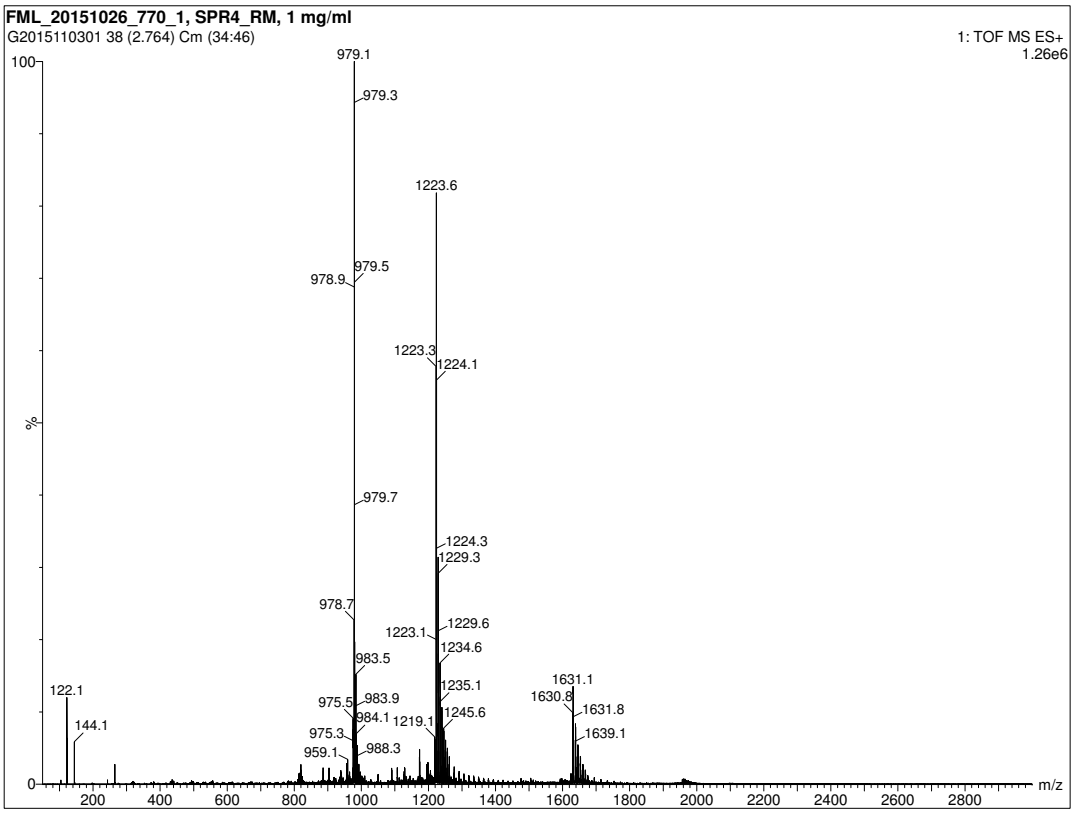

Figure 13. Mass spectra of murikal dissolved in aqueous buffer at Day 0. Average molecular weight= 4891.2 per CoA, major species at $(M+3H)^{3+}/3$= 1631.1, $(M+4H)^{4+}/4$= 1223.6, $(M+5H)^{5+}/5$= 979.1

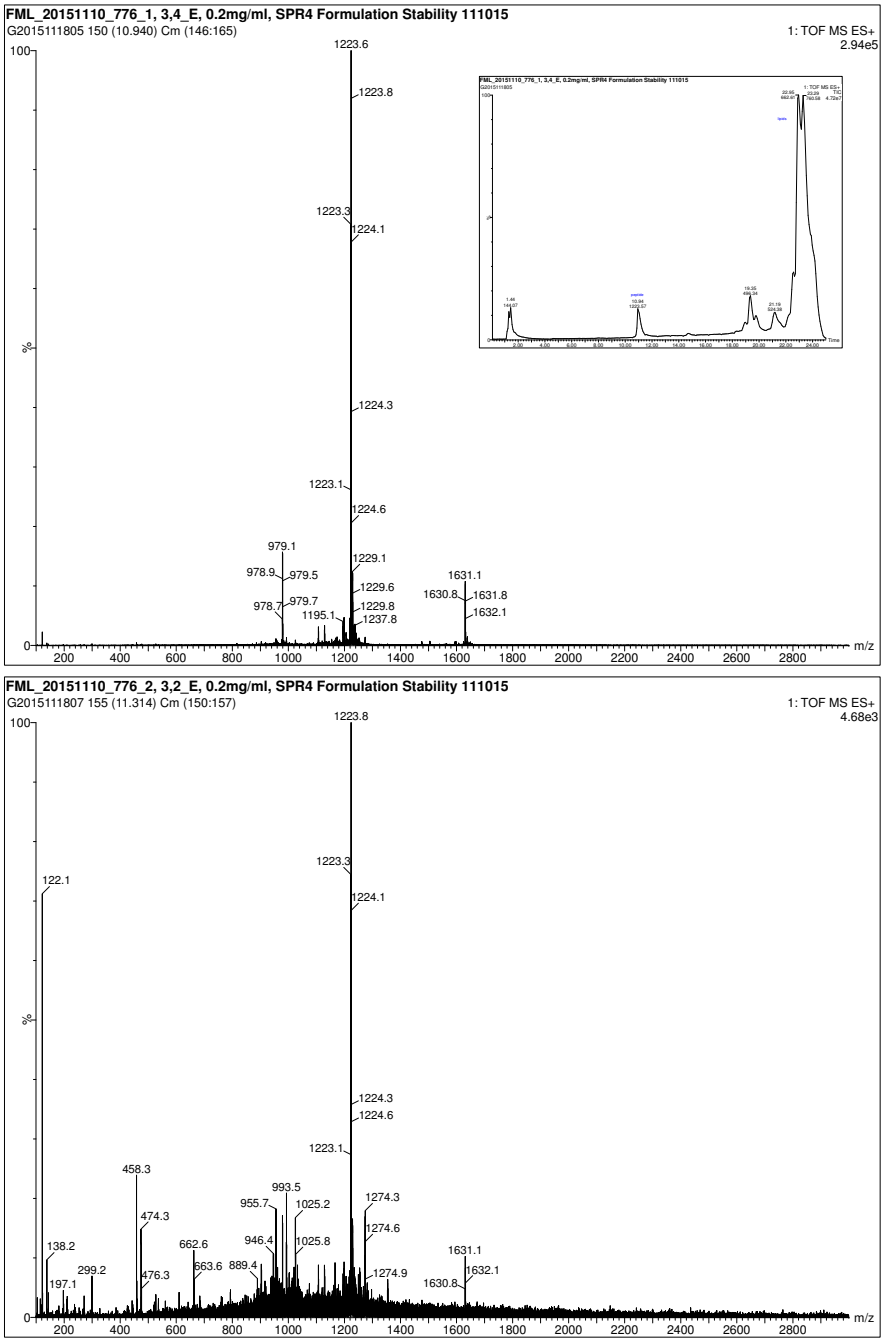

Figure 14. Mass spectra of murikal peptide after one month of storage within liposomal F,3 at 4°C (top) and 25°C (bottom). Mass spectra on peptide associated peak collected at t_R=11 min (LC chromatogram, top insert). Average molecular weight= 4891.2 per CoA, major species at $(M+3H)^{3+}/3$= 1631.1, $(M+4H)^{4+}/4$= 1223.6, $(M+5H)^{5+}/5$= 979.1

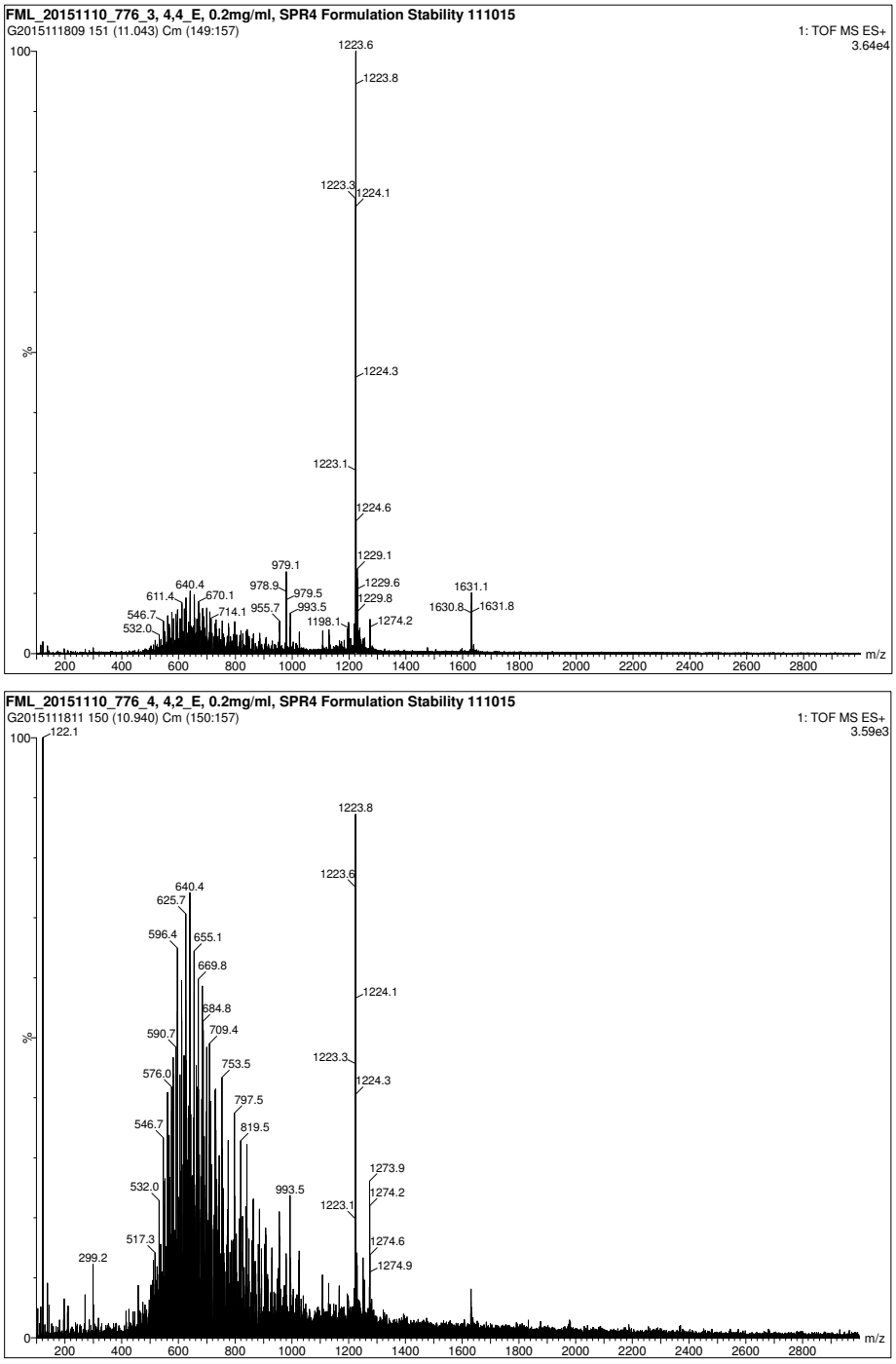

Figure 15. Mass spectra of murikal peptide after one month of storage within liposomal F,4 at 4°C (top) and 25°C (bottom). Average molecular weight= 4891.2 per CoA, major species at $(M+3H)^{3+}/3$= 1631.1, $(M+4H)^{4+}/4$= 1223.6, $(M+5H)^{5+}/5$= 979.1

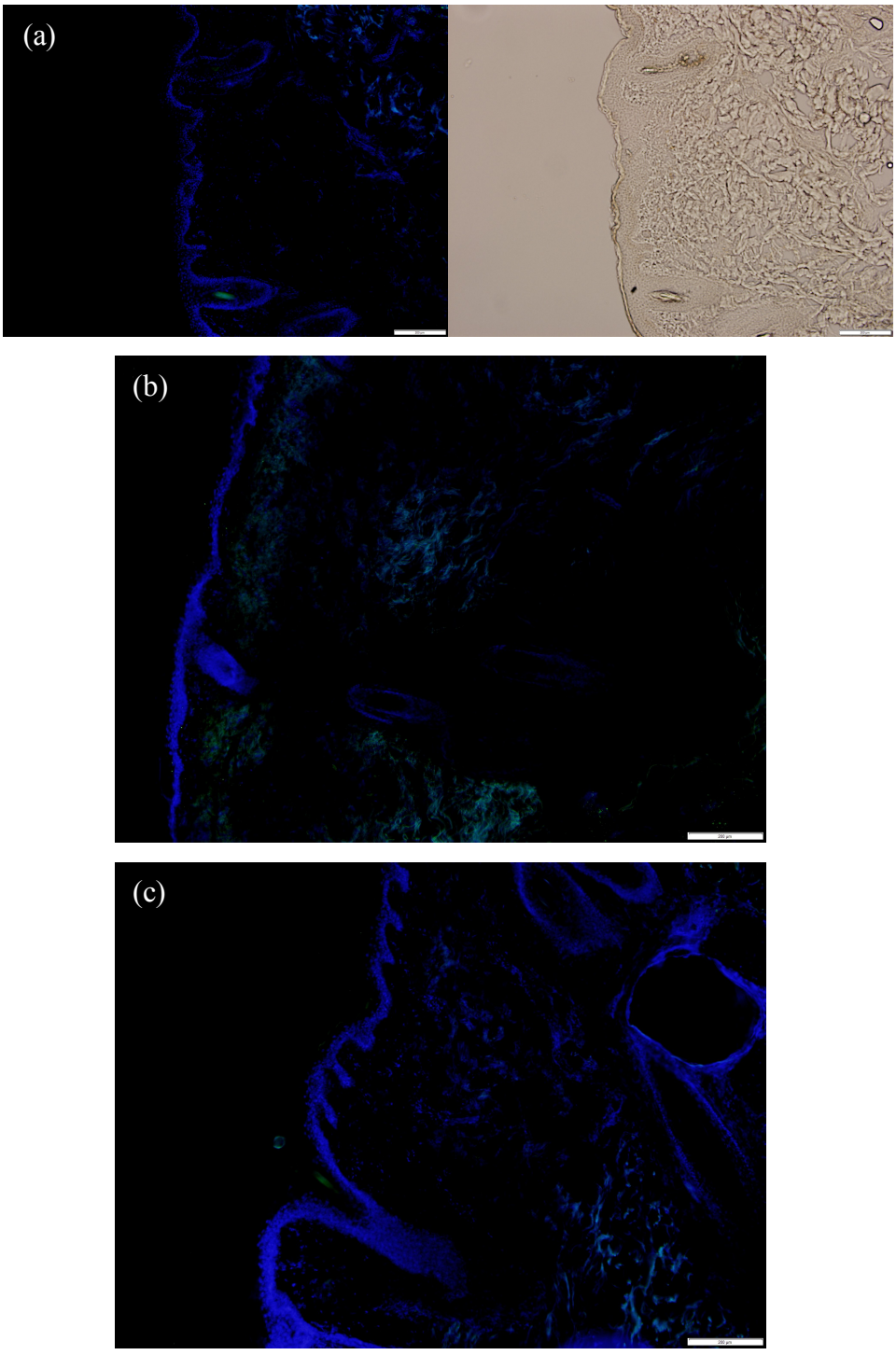

Figure 16. Confocal and light microscope images (10X) of human facial tissue treated with (a) buffer only, (b) F,3 murikal-FITC loaded liposomes and (c) F,4 murikal-FITC loaded liposomes for 30 minutes. Blue; DAPI-Progold stained nuclei and Green; FITC-murikal.

5. Discussion

5.1 Proof of concept: Liposomal topical therapeutic efficacy

Results of F,1 suggested a strong potential for an efficient and targeted topical delivery of the murikal peptide to therapeutically relevant depths of the hair follicle at high concentrations (Figure 4). The hair growth acceleration observed in mice (Figure 5) replicated the observed therapeutic effect of the peptide seen after intradermal injections and also supports the substantial follicular delivery of the peptide within the liposomal formulation. In addition, the observed differences in hair growth rate between mice treated with the murikal formulation and those treated with minoxidil, which showed little effect compared to the controls, reaffirms murikal's considerable therapeutic improvement on current treatment standards As seen in this study and the works adapted, liposomes are a promising tool for topical or transdermal delivery of small and large molecule therapeutics because they are able to encapsulate a wide range of hydrophilic and lipophilic therapeutics due to their amphiphilic composition and due to their membrane structure which serves to easily partition into the lipophilic environments found at the skin surface, dermis and pilosebaceous unit.

5.2 Formulation optimization and *ex-vivo* murine screening

Four additional formulations from successful literature trials of topical delivery of macromolecules were selected to screen against F,1 for optimum dermal penetration and follicle localization of the murikal peptide in its progression towards a human AGA and CIA therapy candidate.

Again following application to depilated mice skin and visualizing with confocal microscopy (Figure 7), F,3 and F,4 were identified as the most optimum due to their extensive murikal (red) dermal penetration and follicle localization. The particular success of F,3 and F,4 can likely be attributed to a number of factors identified in the characterization of the particles in Table 2. Like all other second generation formulations, F,3 and F,4 contained the cationic lipid 1,2-dioleoyl-3-trimethylammonium-propane, (DOTAP) (chloride salt), which according to previous studies[25] and results in Table 2 enhanced the zeta potential and thus particle stability to varying degrees above that of the first generation colloid. Zeta potential, measured in this study through phase analysis light scattering (PALS), represents the charge between the solid surface of a particle and the liquid solution. Zeta potential values > ±30 mV is the accepted threshold to preventing particle aggregation due to charge repulsion effects. In the particular case of F3 which had a measured zeta potential of 74.25 ± 10.03 mV, apparent increase in charge may have acted to stabilize particles through application and absorption into the dermis for optimal follicular delivery. Follicular localization of the positively charged particles may also be attributed to the anionic environment of the skin surface and hair itself leading to promotion of absorption through ion pairing mechanisms.[25]

The enhanced dermal penetration and follicular localization of F3 may also be attributed to its effective diameter which was measured at 237 ±18 nm with a relatively monodisperse, low polydispersity index of 0.29, particle population compared to F,1 which measured at a slightly larger particle diameter of 731 ± 16 nm. Previous studies[33] have indicated an optimum particle diameter in the hundreds of nanometer range for follicle delivery and storage.

The success of F,4 as defined by visual follicle localization in confocal images is harder to substantiate in that its charge is largely neutral and its particle size is well above 1 μm. It is likely that if additional images were available for the similar, ethanol included, F,5, particularly images showing longitudinal sectioning of the pilosebaceous unit instead of latitudinal sectioning as seen in the images provided for F,4, near identical efficacy would be observed. However, it is apparent in the Figure 7 confocal images of F,3 and F,4 that optimum follicle penetration depth is achieved using the smaller, cationic F,3 liposomal formulation. Reaching this target depth at or near the previously discussed bulb region where active keratinocyte proliferation occurs on the surface of the dermal papilla and thus hair growth induction may be critical to achieving an improved therapeutic effect.

5.3 Lead formulations particle and peptide stability

Time and temperature dependent colloidal stability analysis of the lead formulations as observed through measurement of peptide encapsulation efficiency, particle size and zeta potential indicate clear differences in the integrity of the lipid nanoparticle carrier. F,3 was observed to gradually increase its encapsulation of peptide at 4°C and 25°C with the former approaching 86% (m/m) and the latter 100% (m/m) encapsulation by the end of the trial. Similarly, F,4 was observed to also increase its encapsulation of the murikal peptide over the month long study at both storage temperatures with each approaching 100% by trial's end. Total peak area for all formulations at each storage temperature was observed to decrease over time as expected by either peptide precipitation or degradation. However, this decline cannot explain the measured increases in peptide uptake within the lipid phase of the system, particularly

measured values averaging above 100% (m/m) when done in triplicate. These results suggest possible systematic errors in the method development, sample preparation, or chromatogram integration. Although errors may exist in accurate quantification of this particle characteristic, relative conclusions may be drawn on the particles ability to encapsulate a majority of stable peptide into the lipid phase of the liposome formulation over a month of storage at the room temperature (25°C) and refrigerated (4°C) storage conditions.

Dynamic light scattering analysis (DLS) is a common method for measuring particle size and size distribution of a liposome populations. The DLS particle sizing range is a topic of continued debate, but its diameter accuracy is generally accepted from the low nanometer range to near one micron or higher depending on particle density and other factors such as sedimentation rate. The initial mean effective diameter of F,3 was near 300 nm while that of formulation 4 was greater than 2 μm. Polydispersity of both formulations initially suggest that formulation 3 is comprised of a much more monodisperse population of particles (PDI=0.29) compared to that of F,4 which had a PDI of 0.41. This difference in distribution is clearly visualized in the logonormal probability distributions across batches of both formulations at Day 0 and Day 35 after storage at the specified temperatures (Figure 10). Although the accuracy of particle sizing above 1 μm using DLS is highly sample dependent, particularly in the case of a more polydisperse or multimodal sample population such as that found in F,4, relative interpretation of the results can still be made. The liposomes found in F,3 showed near constant 300 nm mean effective diameter with relatively narrow population distributions when stored at both 4°C and 25°C over one month. F,4 DLS data indicated a particle at or

above 1 μm in effective diameter with a wide, heterogeneous population distribution with similar consistency throughout the one month trial period at both 4°C and 25°C. This data indicates both formulations are of stable nature when tracking size while stored at various temperatures over a one month period. However, with optimum particle diameters defined in the hundreds of nanometers[33] for follicle delivery at therapeutically relevant depths and questionable DLS data quality indicating possible particle aggregation or increased sedimentation rates of F,4, F,3 should be considered as the much more stable, definable, and therapeutically optimum based on particle size.

As discussed previously, zeta potential is related to the charge between a particulate surface and its liquid suspension. Ideal values are greater than ±30 mV in that higher charged systems should cause self-repulsion of similar charges leading to decreased particle aggregation and thus higher stability. Again F,3 is indicative of a more stable system in this regard due to its higher, about 70 mV, zeta potential measurements throughout the study at both 4°C and 25°C. Inversely, F,4 measured near neutral at both temperatures throughout the study beyond the final Day 35 reading which measured a zeta potential of nearly 70 mV. This strong fluctuation in measurements could be attributed to a drastic change in surface charge and thus colloidal stability against aggregation, but more likely an explanation is due again to the high polydispersity and sedimentation rate of the F,4 population which can lead to large variations in zeta potential measurements. These results again suggest a greater shelf stability and consistently definable characteristics of F,3 over F,4.

Overall parent peptide was observed in both formulations at the two temperatures tested. Qualitatively significant amounts of the three charged states of the peptide were

deconvoluted to the monoisotopic weight of the parent peptide (not shown). Decreases in peptide associated peak area, particularly for formulations stored at 25°C, indicate a loss of total mass, but particular oxidative or hydrolytic degradants could not be identified using this analysis in the immediate vicinity of the peptide associated peak. This is further supported by the overall loss in spectra intensity from the parent peptide (Figure 13), with further decreases found within the 25°C samples. This analysis indicates an overall presence of parent peptide within both formulations after 40 days of storage at 4°C and 25°C, but apparent increases in the remaining parent peptide in the formulations stored at 4°C point to it's inherent optimal storage temperature.

5.4 Human *ex-vivo* peptide follicle penetration analysis

Following analysis of a single application of both F,3 and F,4 for 30 minutes, confocal images presented in Figure 16 suggest insignificant amounts of murikal penetrated into the human dermis and follicle. However, no peptide was visualized at the surface of the tissue as seen previously in confocal images of treated mice (Figure 4 and Figure 7). This lack of unpenetrated peptide at the tissue surface suggests a possibility of inadequate visualization, which is supported by the change from the 100% (m/m) labeled-peptide applied to the tissues in Figure 4 and 7 to the 3 % (m/m) applied to the human tissue in Figure 16. Application of 100% (m/m) labeled-peptide as done in previous studies is thus needed to unequivocally confirm the failure of these formulations to deliver the therapeutic peptide to the follicle of human tissue. In addition, poor nuclear staining of the human tissue seen in Figure 16 as compared to previous studies needs to be addressed either with additional analysis of cryosectioned tissue, optimization of

DAPI nuclear staining time, or if significant cell death occurred in the time following excision and treatment, alterations in tissue handling or equilibration.

6. Conclusions

In this study, follicular delivery of a promising peptide therapeutic was accomplished through a liposomal topical formulation. The formulation's ability to partition peptide into the dermis and localize within the follicles was visualized using confocal microscopy in a mouse model. Tremendous therapeutic potential was shown in a mouse model, where mice treated with murikal in a liposomal vehicle showed a clear increase in hair growth rate and density over a two week period compared to the leading treatment standard, daily topical murikal applications. Additional formulations were developed and tested to optimize these effects and two were advanced into a month-long stability trial. Although F,4 showed generally reliable stability characteristics, F,3 was determined to be the optimal particle in that it efficiently encapsulated the peptide, had ideal particle size and narrow distribution, and had stable highly charged particle surfaces that counter flocculation. F,3 stored at 4°C also showed an optimal chemical stability of peptide according to mass spectra data. Translation of the efficient topical delivery of the murikal peptide to human hair follicles was not shown conclusively in the first trial.

7. Future Work

Confirming the translatability of the successful delivery of the murikal peptide to human follicles is critical to the eventual therapeutic use of this peptide, particularly within a liposomal formulation. If the peptide can be visualized at or near the levels seen

in the murine confocal studies, further optimizations of the formulation can be made including addition of thickening agents, preservatives and fragrances to make a more marketable product prior to *in vivo* human efficacy trials. Additional studies should also be performed utilizing ZnCl within the formulation as the presence of this metallic ion has previously shown increased bone mineralization activity, which may translate in its hair growth induction.[12]

8. References

1. Blume-Peytavi, U., Whiting, D.A. & Trüeb, R.M. (eds.) Hair Growth and Disorders, Edn. 1. (Springer-Verlag Berlin Heidelberg, 2008).
2. Trueb, R.M. Chemotherapy-induced alopecia. *Curr Opin Support Palliat Care* **4**, 281-284 (2010).
3. Stough, D., Stenn, K., Haber, R., Parsley, W.M., Vogel, J.E., Whiting, D.A. & Washenik, K. Psychological effect, pathophysiology, and management of androgenetic alopecia in men. *Mayo Clin Proc* **80**, 1316-1322 (2005).
4. Sinclair, R. Male pattern androgenetic alopecia. *BMJ* **317**, 865-869 (1998).
5. Rook, A. Endocrine Influences on Hair Growth. *Br Med J* **1**, 609-614 (1965).
6. Rittmaster, R.S., Uno, H., Povar, M.L., Mellin, T.N. & Loriaux, D.L. The effects of N,N-diethyl-4-methyl-3-oxo-4-aza-5 alpha-androstane-17 beta-carboxamide, a 5 alpha-reductase inhibitor and antiandrogen, on the development of baldness in the stumptail macaque. *J Clin Endocrinol Metab* **65**, 188-193 (1987).
7. Jain, B., Singh, B., Katare, O.P. & Vyas, S.P. Development and characterization of minoxidil-loaded liposomal system for delivery to pilosebaceous units. *J Liposome Res* **20**, 105-114 (2010).
8. Kaufman, K.D., Olsen, E.A., Whiting, D., Savin, R., DeVillez, R., Bergfeld, W., Price, V.H., Van Neste, D., Roberts, J.L., Hordinsky, M., Shapiro, J., Binkowitz, B. & Gormley, G.J. Finasteride in the treatment of men with androgenetic alopecia. Finasteride Male Pattern Hair Loss Study Group. *J Am Acad Dermatol* **39**, 578-589 (1998).
9. Monti, D., Tampucci, S., Burgalassi, S., Chetoni, P., Lenzi, C., Pirone, A. & Mailland, F. Topical formulations containing finasteride. Part I: in vitro permeation/penetration study and in vivo pharmacokinetics in hairless rat. *J Pharm Sci* **103**, 2307-2314 (2014).
10. Tampucci, S., Burgalassi, S., Chetoni, P., Lenzi, C., Pirone, A., Mailland, F., Caserini, M. & Monti, D. Topical formulations containing finasteride. Part II: determination of finasteride penetration into hair follicles using the differential stripping technique. *J Pharm Sci* **103**, 2323-2329 (2014).
11. Shin, H., Jo, S.J., Kim do, H., Kwon, O. & Myung, S.K. Efficacy of interventions for prevention of chemotherapy-induced alopecia: a systematic review and meta-analysis. *Int J Cancer* **136**, E442-454 (2015).
12. Martin, A., David, V., Laurence, J.S., Schwarz, P.M., Lafer, E.M., Hedge, A.M. & Rowe, P.S. Degradation of MEPE, DMP1, and release of SIBLING ASARM-peptides (minhibins): ASARM-peptide(s) are directly responsible for defective mineralization in HYP. *Endocrinology* **149**, 1757-1772 (2008).
13. Zelenchuk, L.V., Hedge, A.M. & Rowe, P.S. PHEX mimetic (SPR4-peptide) corrects and improves HYP and wild type mice energy-metabolism. *PLoS One* **9**, e97326 (2014).
14. Zelenchuk, L.V., Hedge, A.M. & Rowe, P.S. SPR4-peptide alters bone metabolism of normal and HYP mice. *Bone* **72**, 23-33 (2015).
15. Atkins, G.J., Rowe, P.S., Lim, H.P., Welldon, K.J., Ormsby, R., Wijenayaka, A.R., Zelenchuk, L., Evdokiou, A. & Findlay, D.M. Sclerostin is a locally acting regulator of late-osteoblast/preosteocyte differentiation and regulates

mineralization through a MEPE-ASARM-dependent mechanism. *J Bone Miner Res* **26**, 1425-1436 (2011).
16. Rowe, P.S. Regulation of bone-renal mineral and energy metabolism: the PHEX, FGF23, DMP1, MEPE ASARM pathway. *Crit Rev Eukaryot Gene Expr* **22**, 61-86 (2012).
17. David, V., Martin, A., Hedge, A.M. & Rowe, P.S. Matrix extracellular phosphoglycoprotein (MEPE) is a new bone renal hormone and vascularization modulator. *Endocrinology* **150**, 4012-4023 (2009).
18. Watt, F.M. Epidermal stem cells: markers, patterning and the control of stem cell fate. *Philos Trans R Soc Lond B Biol Sci* **353**, 831-837 (1998).
19. Lauer, A.C., Ramachandran, C., Lieb, L.M., Niemiec, S. & Weiner, N.D. Targeted delivery to the pilosebaceous unit via liposomes. *Adv. Drug Deliv. Rev* **18**, 311-324 (1996).
20. Ciotti, S.N. & Weiner, N. Follicular liposomal delivery systems. *J Liposome Res* **12**, 143-148 (2002).
21. Niemiec, S.M., Ramachandran, C. & Weiner, N. Influence of nonionic liposomal composition on topical delivery of peptide drugs into pilosebaceous units: an in vivo study using the hamster ear model. *Pharm Res* **12**, 1184-1188 (1995).
22. Lieb, L.M., Flynn, G. & Weiner, N. Follicular (pilosebaceous unit) deposition and pharmacological behavior of cimetidine as a function of formulation. *Pharm Res* **11**, 1419-1423 (1994).
23. Saffari, M., F, H.S., Oghabian, M.A. & Moghimi, H.R. Preparation and in-vitro Evaluation of an Antisense-containing Cationic Liposome against Non-small Cell Lung Cancer: a Comparative Preparation Study. *Iran J Pharm Res* **12**, 3-10 (2013).
24. Kim, S.T., Lee, K.M., Park, H.J., Jin, S.E., Ahn, W.S. & Kim, C.K. Topical delivery of interleukin-13 antisense oligonucleotides with cationic elastic liposome for the treatment of atopic dermatitis. *J Gene Med* **11**, 26-37 (2009).
25. Jung, S., Otberg, N., Thiede, G., Richter, H., Sterry, W., Panzner, S. & Lademann, J. Innovative liposomes as a transfollicular drug delivery system: penetration into porcine hair follicles. *J Invest Dermatol* **126**, 1728-1732 (2006).
26. Han, I., Kim, M. & Kim, J. Enhanced transfollicular delivery of adriamycin with a liposome and iontophoresis. *Exp Dermatol* **13**, 86-92 (2004).
27. Shariat, S., Badiee, A., Jaafari, M.R. & Mortazavi, S.A. Optimization of a Method to Prepare Liposomes Containing HER2/Neu- Derived Peptide as a Vaccine Delivery System for Breast Cancer. *Iran J Pharm Res* **13**, 15-25 (2014).
28. Verma, D.D. & Fahr, A. Synergistic penetration enhancement effect of ethanol and phospholipids on the topical delivery of cyclosporin A. *J Control Release* **97**, 55-66 (2004).
29. Rao, Y., Zheng, F., Zhang, X., Gao, J. & Liang, W. In vitro percutaneous permeation and skin accumulation of finasteride using vesicular ethosomal carriers. *AAPS PharmSciTech* **9**, 860-865 (2008).
30. Szoka, F., Jr. & Papahadjopoulos, D. Procedure for preparation of liposomes with large internal aqueous space and high capture by reverse-phase evaporation. *Proc Natl Acad Sci U S A* **75**, 4194-4198 (1978).

31. Jaafar-Maalej, C., Diab, R., Andrieu, V., Elaissari, A. & Fessi, H. Ethanol injection method for hydrophilic and lipophilic drug-loaded liposome preparation. *J Liposome Res* **20**, 228-243 (2010).
32. Niemiec, S.M., Latta, J.M., Ramachandran, C., Weiner, N.D. & Roessler, B.J. Perifollicular transgenic expression of human interleukin-1 receptor antagonist protein following topical application of novel liposome-plasmid DNA formulations in vivo. *J Pharm Sci* **86**, 701-708 (1997).
33. Lademann, J., Richter, H., Schanzer, S., Knorr, F., Meinke, M., Sterry, W. & Patzelt, A. Penetration and storage of particles in human skin: perspectives and safety aspects. *Eur J Pharm Biopharm* **77**, 465-468 (2011).